

# Parenclitic hypergraphs and their application in personalized cancer therapy

K. K. H. Manjunatha,<sup>1,\*</sup> D. Aleja,<sup>2,\*</sup> F. Liu,<sup>3,\*</sup> M. Zhang,<sup>4,\*</sup> Y. Qi,<sup>5</sup> L. Minati,<sup>6,7,8,†</sup> G.-Q. Sun,<sup>9,10,‡</sup> S. Zhuang,<sup>11</sup> C. Cai,<sup>4</sup> J. Li,<sup>12</sup> R. Criado,<sup>2</sup> M. Romance del Rio,<sup>2</sup> D. Papo,<sup>13,14</sup> Y.-J. Ma,<sup>15,16</sup> F. Fang,<sup>6</sup> C. I. del Genio,<sup>9,6,17,18</sup> Z. Zhao,<sup>17</sup> H. Gao,<sup>3,§</sup> and S. Boccaletti<sup>6,9,17,19,¶</sup>

<sup>1</sup>*Scuola Superiore Meridionale, Modeling and Engineering Risk and Complexity Program, Via Mezzocannone 4, 80138 Napoli, Italy*

<sup>2</sup>*Universidad Rey Juan Carlos, 28933 Móstoles, Madrid, Spain*

<sup>3</sup>*Research Institute of Intelligent Control and Systems, Harbin Institute of Technology, 92 Xidazhi Street, Nangang District, 150001 Harbin, China*

<sup>4</sup>*Key Laboratory of Systems Health Science of Zhejiang Province, School of Life Science, Hangzhou Institute for Advanced Study, University of the Chinese Academy of Sciences, 310024 Hangzhou, China*

<sup>5</sup>*Research Institute of Intelligent Control and Systems, Harbin Institute of Technology, Harbin 150001, China*

<sup>6</sup>*International Research Center of Complexity Sciences,*

*Hangzhou International Innovation Institute, Beihang University, Hangzhou 311115, China*

<sup>7</sup>*School of Life Science and Technology, University of Electronic Science and Technology of China, 611731 Chengdu, China*

<sup>8</sup>*Center for Mind/Brain Sciences (CIMEC), University of Trento, 38123 Trento, Italy*

<sup>9</sup>*School of Mathematics, North University of China, 3 Xueyuan Road, Shanglan Jiancaoping District, 030051 Taiyuan, China*

<sup>10</sup>*Complex Systems Research Center, Shanxi University,*

*92 Wucheng Road, Xiaodian District, 030006 Taiyuan, China*

<sup>11</sup>*Research Center of Intelligent Control and Systems, Yongjiang Laboratory, 1792 Cihai South Road, Zhenhai District, 315202 Ningbo, China*

<sup>12</sup>*Department of Thyroid and Breast Surgery, Zhongnan Hospital of Wuhan University, 169 Donghu Rd, Wuchang District, 430071 Wuhan, China*

<sup>13</sup>*Fondazione Istituto Italiano di Tecnologia, Ferrara, Italy*

<sup>14</sup>*Department of Neuroscience and Rehabilitation, University of Ferrara, Ferrara, Italy*

<sup>15</sup>*School of Business, East China University of Science and Technology,*

*130 Meilong Road, Xuhui District, 200237 Shanghai, China*

<sup>16</sup>*Research Center for Econophysics, East China University of Science and Technology, 130 Meilong Road, Xuhui District, 200237 Shanghai, China*

<sup>17</sup>*Institute of Interdisciplinary Intelligent Science,*

*Ningbo University of Technology, Ningbo 315211, China*

<sup>18</sup>*MU Pleven, Ul. Sv. Kliment Ohridski 1, Pleven, 5800, Bulgaria*

<sup>19</sup>*CNR - Institute of Complex Systems, Via Madonna del Piano 10, I-50019 Sesto Fiorentino, Italy*

(Dated: July 7, 2026)

Understanding the differences between individual instances of the same complex system remains a central challenge, particularly in biological contexts. Parenclitic networks constitute a suitable means to detect deviations in correlations with respect to reference populations. Here, we introduce parenclitic hypergraphs, a general framework for identifying anomalies in higher-order correlations across arbitrary interaction orders. After validating the method on synthetic datasets and benchmark ones, we apply it to patient-derived cancer organoids, capturing temporal changes in gene expression between healthy and cancerous tissues as the disease progresses. Our approach not only reproduces known oncogenic signatures, but also reveals a previously unrecognized candidate therapeutic target. Since organoids are generated from individual patients, our method provides, for the first time, a viable protocol for personalized cancer therapy based on higher-order correlation patterns. These findings offer a novel, systems-level strategy for precision oncology grounded in complex systems theory.

## I. SIGNIFICANCE STATEMENT

Complex systems are in general governed by coordinated changes involving multiple variables simultaneously, yet most data analysis methods focus only on individual variables or pairwise relationships. We introduce parenclitic hypergraphs, a general framework that captures higher-order deviations from normal behavior without requiring prior assumptions about which inter-

\* These authors contributed equally to the manuscript.

† Corresponding author: lminati@uestc.edu.cn

‡ Corresponding author: gquansun@126.com

§ Corresponding author: hjgao@hit.edu.cn

¶ Corresponding author: stefano.boccaletti@gmail.com

actions are important. By representing samples through weighted group relationships, our method uncovers informative patterns that remain invisible to conventional studies. Tests on synthetic and benchmark datasets demonstrate substantial gains in feature discovery. Applied to patient-derived breast-cancer organoids, parenclitic hypergraphs identify patient-specific vulnerabilities, opening new opportunities for personalized medicine via higher-order data analysis.

## II. INTRODUCTION

Most natural and artificial complex systems have a typical underlying structure in which relationships exist between specific pairs of the constituent individual components. Thus, complex networks, which naturally embody this type of connections, have proved to be an invaluable tool to represent them and to investigate phenomena occurring in social, ecological, biological and technological systems [1–4]. As just described, the original paradigm of complex networks is that of a direct mapping of the relationships of pairs of components of a system onto a graph, possibly with the addition of link weights to encode a topological or functional observable associated to them. A question then arises naturally, namely that of how to determine and quantify the general difference between two networks and, thus, between the two systems they represent. A number of approaches have been used to provide methodological answers. In the simplest form, one can compare some structural properties between the networks, such as their degree distribution. However, when trying to relate structure and function, with the ultimate goal of predicting and classifying the behaviour of a given network, such a comparison must account for the variability of the observables within the specific functional classes. Thus, sampling methods are often used to build ensembles of networks with specified characteristics, such as the sequence of node degrees [5–7] or the structure of correlations [8], and to find the typical distribution of their observables, allowing one to assess how much the features of a given network deviate from their expected values [9]. This approach, however, presupposes the possibility to precisely detect the structure of a network and the ability of associating some specific structural observable to particular functional features. Unfortunately, these two conditions are not always fulfilled, especially when studying biological systems, where the links in the networks often indicate some type of correlation, and typically have large uncertainties.

A different method that is particularly useful in such cases is that of parenclitic networks [10]. The idea behind this technique is to infer the multidimensional relationship between a set of observed features of a system and their functional behaviour. To do so, one starts by considering a group of  $N$  systems, all belonging to the same functional class. All the systems undergo the same experimental treatment, resulting in a fixed number  $N_f$  of

features being measured on each instance. Thus, each system is represented as a point in an  $N_f$ -dimensional metric space. Note that the method is very general, and it makes no assumption on the type of system or on the nature of the features measured. Next, one projects the  $N$  points obtained on all possible planes, which are  $\binom{N_f}{2} = \frac{N_f(N_f-1)}{2}$  in number. Each such projection represents the implicit relationship between the two features corresponding to the dimensions chosen. Then, one estimates such relationships, obtaining a function that describes them. The specific way to perform these estimates is not prescribed, and one can use anything, from simple techniques such as linear or polynomial regression, to more complex machine-learning algorithms. At this point, one is ready to analyze an unknown system. Once its features have been measured, the system is associated to a complete weighted network in which each node corresponds to a feature, and the weight of the link  $(i, j)$  is the distance between the point representing the system and the estimated function that relates feature  $i$  and feature  $j$  in the  $(i, j)$  projection plane. This procedure is schematically illustrated in Fig. 1(a)–(c). The networks thus built represent the *deviations* of each pair of features from the values expected for the reference population. Thus, they are called *parenclitic networks*, from the ancient Greek *παρέγκλισις*, indicating a random deviation in the trajectory of atoms according to the Epicurean doctrine, especially following the tradition of Lucretius.

Parenclitic networks have proved to possess a remarkable predictive power in multiple areas of research [11–17]. However, their classic formulation carries the intrinsic limitation of only accounting for pairwise correlations, resulting, in fact, in a traditional type of network. In the last few years, however, researchers have been increasingly paying attention to the importance of higher-order interactions in complex systems [18, 19]. Once more, the main example of the importance of many-body interactions is offered by biological systems, in which they are a defining feature together with multi-scale correlations. Here, we apply the idea of parenclitic analysis to higher-order interactions, introducing parenclitic hypergraphs, which capture simultaneous relationships amongst multiple features of complex datasets. Because of combinatorial explosion, the method has an inherent scalability problem, which we solve by proposing heuristics whose performance and effectiveness we validate on both synthetic data and real-world benchmarks. Finally, building parenclitic hypergraphs from the gene-expression profiles of a breast cancer patient, we detect new potential therapeutic targets at the level of genes and proteins, demonstrating the applicability of our method in personalized medicine.

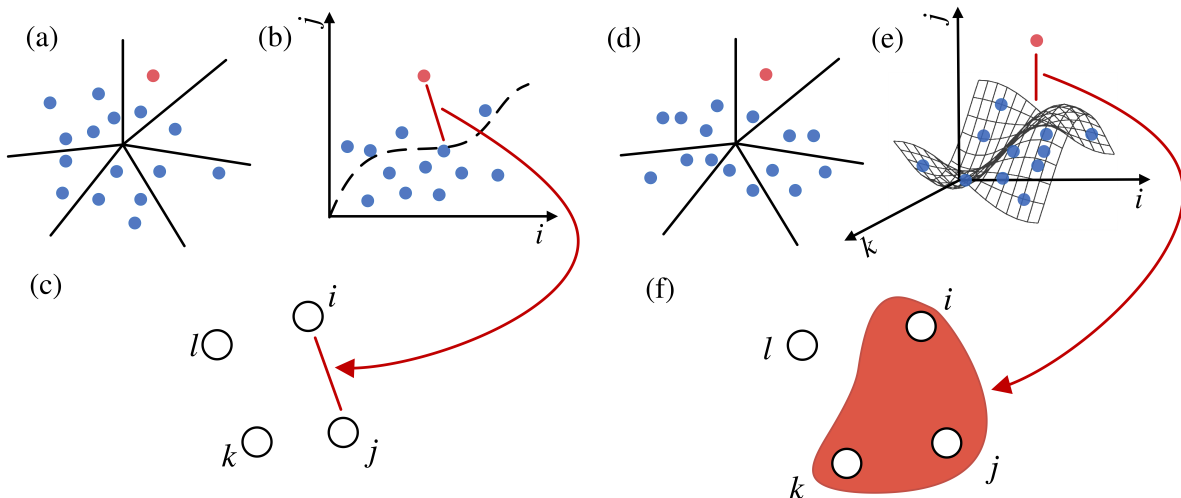


Figure 1. **Parenclitic networks and parenclitic hypergraphs.** (a,d) The initial dataset consists of  $N$  subjects for which  $N_f$  features have been measured. Thus, the subjects can be represented as (blue) points in an  $N_f$ -dimensional space. An extra, unlabelled, system is shown as a red point. (b) The data are projected onto all  $\frac{N_f(N_f-1)}{2}$  possible planes, each having two distinct features  $i$  and  $j$  as axes. In each of these planes, the function that relates the two features is estimated (dashed line), and the distance between the point representing the unlabeled subject and such function (red segment) is computed. (c) The parenclitic network associated to the unlabeled subject is a network where each node corresponds to a feature, and the weight of each link  $(i, j)$  is the distance between the red point and the function in the  $(i, j)$  plane, so that the length of the red segment in panel (b) becomes the weight of the red link in panel (c). (e) For the construction of a parenclitic hypergraphs with three-body correlations, all the data are projected onto all possible 3-dimensional spaces, each having three distinct features  $i, j$  and  $k$  as axes. In each of these spaces, the surface relating the features is estimated, and the distance between the unlabelled subject (red point) and the surface is computed. (f) The parenclitic hypergraph associated to the unlabelled subject is a higher-order network in which each node corresponds to a feature, and the weight of each hyperedge  $(i, j, k)$  is the distance between the red point and the estimated surface in the  $(i, j, k)$  projection space.

### III. RESULTS

#### A. Parenclitic hypergraphs and scalability

To build a parenclitic network that accounts for  $D$ -order correlations from a dataset of  $N$  systems with  $N_f$  features each, one starts by projecting the data points no longer onto planes, but onto spaces of a higher dimension  $D$ . Then, the relationship between the features is inferred not in the form of a line, but rather in the form of a  $D - 1$ -dimensional hypersurface embedded in the chosen space. Thus, for example, one can consider all 3-dimensional spaces, each corresponding to a choice of three different features, and represent the relationships as surfaces within them.

Given an unlabelled system, one then computes the distance between the point that represents it and each of these hypersurfaces. Finally, these distances are assigned as weights to the corresponding hyperedges between the  $D$  nodes representing the specific features chosen for each projection. Note that this procedure, shown in Fig. 1(d)–(f) for  $D = 3$ , results in a  $D$ -uniform weighted hypergraph, as all hyperedges have size  $D$ .

While in principle the construction of a parenclitic hy-

pergraph can be carried out by following the steps just described, it is worth noting that there is a substantial change in complexity between traditional networks and hypergraphs. In fact, in the former case, one has to determine a number of functions of a single variable that is of the order of  $N_f^2$ . However, for a  $D$ -uniform parenclitic hypergraph, this grows to  $N_f^D$  functions of  $D - 1$  variables. Thus, even assuming that the computational complexity of determining each function is a polynomial function of  $N$  and  $D$ , the total complexity of the process can quickly become prohibitive as  $D$  grows. To solve this problem, we introduce an approximation in the calculation of the distance between the point representing the unlabelled system and the hypersurfaces describing the known data points. Specifically, in each  $(i, j, k)$  projection space we compute the Euclidean distances between the unlabelled point and each of the other data points, and take the smallest one as a proxy for the distance with the hypersurface in that space. Computing the distances requires a number of operations that is proportional to  $D$  for each of the  $N$  data points. Thus, the complexity of finding the distances that provide the weights of the hyperedges in the parenclitic hypergraph is  $DN$  for each of the projection spaces, resulting in a

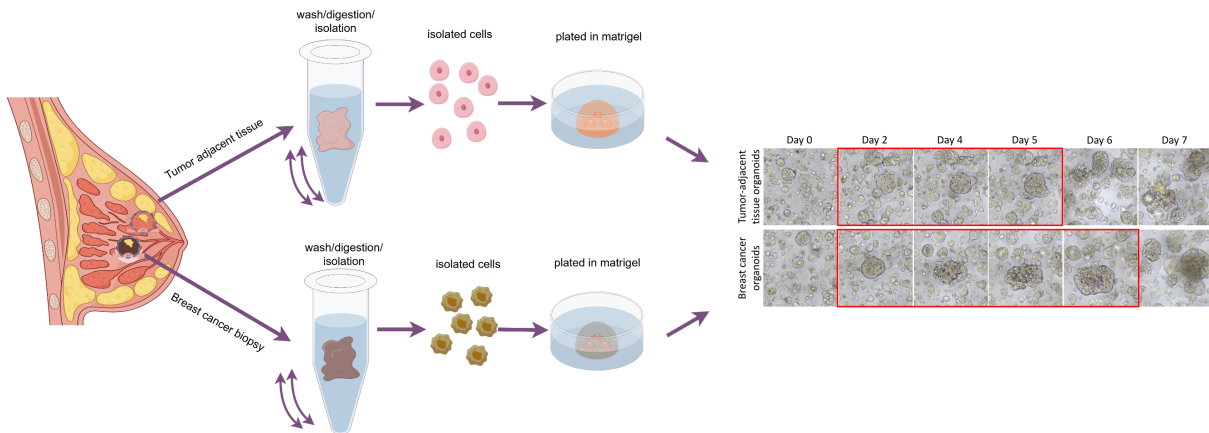


Figure 2. **Illustration of the process of organoid growth.** Tissue samples are taken from the cancer and from tumour-adjacent tissue. Cells are subsequently isolated and seeded in a gel matrix, in which they eventually develop into miniature versions of the original organ, conserving their healthy or pathological properties.

total of the order of  $DNN_f^D$ . But the complexity of estimating a function of  $D - 1$  variables from  $N$  points is certainly greater than  $DN$ , which is already smaller than the lower bound of  $D^2N$  one obtains for the linear case. Thus, this approximation provides a substantially more favourable scaling than would be obtained with the full estimation of the hypersurfaces, which, in turn, makes the use of the method feasible even for a large number of dimensions.

## B. Validation on synthetic data

To provide an initial validation of our method, we first apply it to synthetic data. To this end, we start by constructing a negative population of subjects and a positive one. Each population consists of 1000 subjects, and each subject is described by 10 features  $f_i$ . The features of the subjects in the negative population are uniformly distributed random numbers in the interval  $(0, 1)$ , and, as such, no correlations exist between them. The features of the subjects in the positive population are instead chosen in a way to impose the existence of linear or non-linear correlations between three sets of three features each, namely  $(1, 2, 3)$ ,  $(4, 5, 6)$  and  $(7, 8, 9)$  (for details see the Methods Section V A).

Next, we take all the subjects in the positive population and use them as labelled data points, as described in the previous subsection. Then, for each subject of the negative population, we construct a parenclitic hypergraphs with edges of size 3.

As the next step, we build the average parenclitic hypergraph, in which we give each hyperedge a weight that is the average of the weights it has in the 1000 parenclitic hypergraphs built.

Finally, we repeat the procedure 100 times and average the results over all realizations. The resulting weights of the hyperedges between the correlated triplets are

$\bar{w}_{1,2,3} = 0.239$ ,  $\bar{w}_{4,5,6} = 0.286$  and  $\bar{w}_{7,8,9} = 0.262$  in the linear-correlation case, and  $\bar{w}_{1,2,3} = 0.308$ ,  $\bar{w}_{4,5,6} = 0.293$  and  $\bar{w}_{7,8,9} = 0.262$  in the non-linear one, whereas the mean weight of all other hyperedges is 0.101 in the former case and 0.116 in the latter. Thus, the weights of the hyperedges corresponding to correlated features are always at least twice as large as the mean of the weights of all other hyperedges, regardless of whether the functions chosen were linear or non-linear.

## C. Analysis of real-world datasets

Next, to show how parenclitic hypergraphs can extract information of higher quality with respect to traditional parenclitic networks, we apply the method to 5 known datasets, namely:

1. The Breast Cancer Wisconsin (Diagnostic) Dataset [20, 21], containing the values of features derived from digitized images of fine-needle aspirate samples of breast masses, focusing on the characteristics of the cell nuclei present in the images.
2. The Parkinson's Disease Detection Dataset [22, 23], which is specifically designed for the diagnosis of Parkinson's Disease using voice recordings.
3. The Heart Disease Dataset [24, 25], which includes clinical and demographic attributes used to predict the occurrence of heart disease in patients.
4. The Breast Cancer Coimbra Dataset [26, 27], consisting of anthropometric data and blood-test results of several tens of breast-cancer patients and control-group people.

5. The Indian Liver Patient Dataset [28, 29], which is a clinical dataset used for liver disease diagnosis on patients from the state of Andhra Pradesh in India.

For all datasets, described more in detail in the Methods Section V B, we used the procedures described above, to build traditional parenclitic networks as well as 3-uniform parenclitic hypergraphs, taking the data of the healthy subjects as labelled reference points. From these, we created an average parenclitic network and an average parenclitic hypergraph in which each edge weight is the mean of the weights the same edge has over all the parenclitic networks or hypergraphs, respectively. Thus, if  $\bar{w}_{i,j}$  is the weight of edge  $(i, j)$  in the average parenclitic network and  $\bar{w}_{i,j,k}$  is the weight of hyperedge  $(i, j, k)$  in the average parenclitic hypergraph, the total strength of node  $i$  is

$$k_i^g = \sum_j \bar{w}_{i,j} \quad (1)$$

in the traditional network and

$$k_i^h = \frac{1}{2} \sum_{j,k} \bar{w}_{i,j,k} \quad (2)$$

in the hypergraph case. A comparison between the two can then be carried out in a very straightforward way, as edges and hyperedges can be ranked by their weights in the average networks, and nodes by their total strengths.

The largest differences between the pairwise approach and the higher-order one are observed in the Coimbra breast cancer data and in the Indian liver-patient data. In the former, both methods identify blood glucose levels as the most significant feature. Also, they both find age, serum levels of resistin and of Monocyte Chemoattractant Protein 1 to be within the 5 most important features. However, while the pairwise parenclitic graph points at the serum levels of insulin as a feature of high significance, the higher-order results replace this with body-mass index (BMI) This shows that the higher-order parenclitic network avoids redundancies better than the traditional pairwise one does. In fact, the insulin levels clearly relate the blood glucose values. Thus, including it amongst the most important features is redundant, when the other is already present. The higher-order network, though, replaces insulin with BMI, which a growing body of research correlates with the incidence of breast cancer [30–33].

Similarly, both methods show a strong agreement for three of the top 5 features in the Indian liver-patient dataset, confirming the importance of anomalies in direct bilirubin and alkaline phosphatase, and of age as markers of disease. However, while the pairwise approach identifies total bilirubin and alanine aminotransferase as the other two most important features, the hypergraph one replaces them with total protein and serum levels of albumin. Once more, this shows that the higher-order method is less prone to provide redundant results, since the total bilirubin and direct bilirubin are clearly related,

and are thus replaced by total levels of proteins and altered levels of albumin, providing a heightened precision in the detection of the most relevant alterations for a diagnosis.

#### D. Personalized medicine application

Having demonstrated that parenclitic hypergraphs correctly detect higher-order correlations in complex datasets and provide highly detailed information about their structure, we applied the method to the case of a breast cancer patient, with the goal of detecting possible therapeutic targets for the specific individual.

To do so, we started from tissues excised during a mastectomy and grew pathological organoids from cancerous tissue and clinically healthy ones from tumor-adjacent tissue, as sketched in Fig. 2 and detailed in the Methods Section V C. Organoids are effectively a miniature version of a whole organ, which means that they retain much of the structural and functional complexity of the original tissue [34]. Also, growing them from cells harvested from a patient allows us to infer conclusions that are specific to the pathology as it manifests in that particular person.

Subsequently, we used two different approaches to construct parenclitic networks of the gene expression levels of the organoids (for details of RNA sequencing, see the Methods Section V D). First, we considered the data from each day of the healthy organoids as the reference points, building one parenclitic graph and one parenclitic hypergraph for each day from the data of the cancer organoids. This enables a comparison between the correlations of the cancer gene networks and those of a healthy organ. Then, we constructed parenclitic networks for each day of the cancer organoids, using the other 6 days as reference, to uncover how the deviations in gene expression correlations change in time. Finally we ranked the genes by their total strength, extracting in each case the top 15 genes for comparative analysis. As an illustrative example, in Fig. 3 we report the expression levels over time of 19 notable genes identified by our method, whose relevance is discussed below.

##### 1. Comparing cancer with clinically healthy tissue

The results once more show that, when comparing clinically healthy tissue with cancer, the higher-order method yields less redundancy than the traditional pairwise one. In fact, both methods identify mostly genes and gene families that are associated with cancer and, often, used as cancer markers. Additionally, a smaller number of genes whose functions relate to the cell respiratory chain, immune reaction, cell organization and the formation of connective tissue are also detected as relevant. However, while the two methods find a number of common genes, the results also have some significant differences. In par-

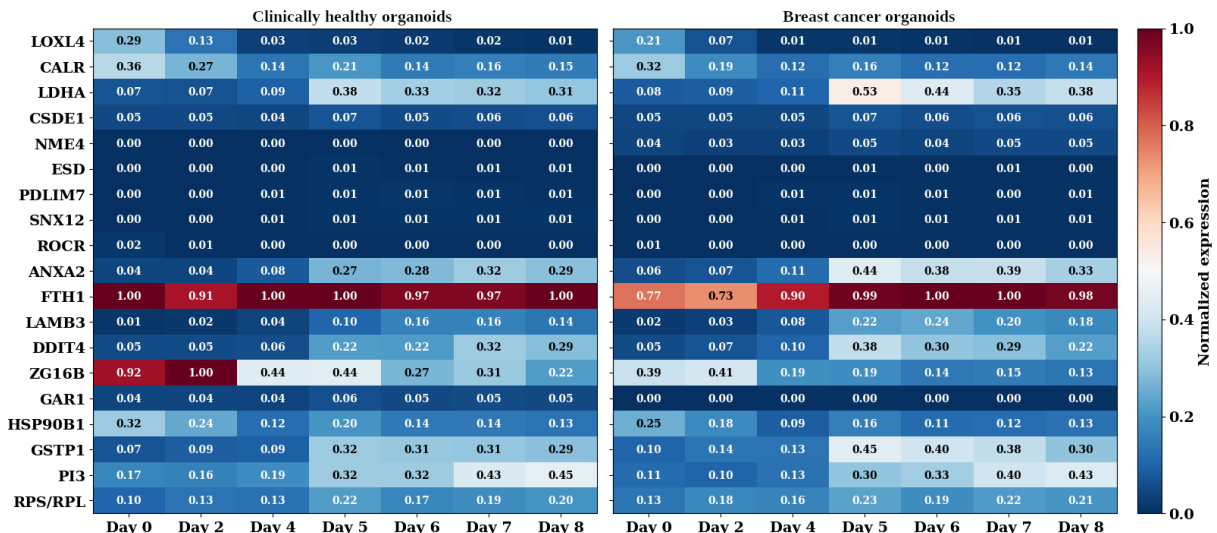


Figure 3. **Temporal expression patterns of the main 19 genes identified by parenclitic networks.** The heatmaps show the expression levels of a set of 19 biologically relevant genes across seven time points in clinically healthy organoids (left) and cancer organoids (right). To enable direct visual comparison between the two conditions, gene expression values from both datasets were jointly normalized using a unified min-max scaling. As a result, identical colour intensities correspond to the same absolute expression levels across both heatmaps. Each cell in the heatmap is annotated with its normalized expression value, facilitating quantitative inspection in addition to qualitative pattern recognition. The RPS/RPL row represents the mean expression of all ribosomal protein genes identified in the union gene set, summarizing the collective translational activity over time. Note that the top genes do not correspond necessarily to those that are overexpressed or underexpressed, since the method detects alterations in the relations between expression levels.

ticular, the pairwise network identifies 3 genes that are excluded by the higher-order one. These are:

- LOXL4, which is responsible for encoding the protein *lysyl oxidase like 4* and has been recently found to promote cell outgrowth in breast cancer [35];
- CALR, which encodes *calreticulin*, which is known to be the principal signaling molecule for the immune system to attack cancer cells [36];
- LDHA, which encodes one of the units of *lactate dehydrogenase* and that has long been known to be a marker for cancer and an indicator of poor prognosis [37].

Conversely, a number of genes are only detected as relevant by the higher-order method:

- CSDE1, encoding *cold shock domain protein E1*, which plays a fundamental role as a regulator of gene expression in cancer [38, 39];
- NME4, which encodes *protein expressed in non-metastatic cells 4*, known to be overexpressed in many cancers and thought of as part of the immune reaction to inhibit metastasis formation [40];
- ESD, which encodes *esterase D* and that is considered a non-specific cancer marker [41–43];

- PDLIM7, encoding *PDZ-and-LIM domain protein 7*, which some studies suggest may promote cancer progression [44];
- SNX12, which encodes *sorting nexin 12*, which belongs to a family whose altered level of expression have been associated to cancer [45];
- ANXA2, which encodes *annexin II*, which is a regulator of cell growth and has long been associated with the epithelial-mesenchymal transition that initiates metastatic spread of tumours [46].
- ROCR, encoding *regulator of chondrogenesis RNA*, which has been recently found to be related to overexpression of the SOX9 transcription factor, which, in turn, is related to highly aggressive forms of breast cancer via the control of the expression of a number of co-factors, including, mainly, L-SOX5a and SOX6 [47–49];

The difference between the results obtained with the two methods clearly demonstrates the additional information one can obtain by studying correlations beyond pairwise ones. This is particularly evident in the case of ROCR, whose relevance for cancer growth is strong and known, but is not captured by the pairwise network because its effect is mediated by a two-step interaction.

## 2. Temporal evolution of cancer network

Finally, the results comparing the correlations in expression levels for each day of the cancer with the other days used as a reference offer a different perspective about the genes that may be fundamental for the progression of the disease. In fact, also in this case the pairwise network and the higher-order one present similarities and differences in the genes that are identified. It is, however, from their detailed analysis that we can highlight the potential of our method in finding new therapeutic targets.

In particular, some of the genes that are detected as relevant solely by the pairwise approach are also identified by the comparison of cancer tissue with healthy tissue. These are CALR, whose function we discussed above, the eEF family, which are known breast cancer markers, and the ATP synthase family, with the last two that, in the previous comparison, are found by both the pairwise and the higher-order method. Additionally, three more genes are only detected by the pairwise method, namely:

- FTH1, which encodes *ferritin heavy chain*, whose function is to act as the main intracellular iron storage protein, and whose disruption has been associated with breast cancer [50];
- LAMB3, encoding the  $\beta$ -3 subunit of *laminin*, which is a protein that is necessary for the formation and function of basement membranes, which are most often disrupted by cancer progression and, as such, has been considered as a generic cancer marker [51];
- DDIT4, which encodes *DNA-damage-inducible transcript 4*, and is likely to be a reaction to the proliferation of cancer cells, since it downregulates the mTOR protein, which, in turn, is deregulated in a large number of cancers [52–54].

Similarly, several genes are only detected when analyzing the higher-order parenclitic network. One of them is LOXL4, which we discussed above. Moreover, we find:

- RPS/RPL family, also detected in the other comparison at both orders, which is responsible for ribosome formation and is overexpressed in several cancers [55];
- ZG16B, encoding *zymogen granule protein 16b*, whose upregulation is associated to breast cancer [56, 57];
- GAR1, which encodes *H/ACA ribonucleoprotein complex subunit 1* and that indirectly re-activates the core reverse transcriptase of the human telomerase complex, a condition that is found in the almost totality of cancers [58].

In addition to those described above, the use of parenclitic networks reveals three more genes that appear to be of particular therapeutic interest. The first, detected at

both orders of interaction on day 2, is HSP90B1, encoding the *Heat shock protein 90kDa beta member 1*, which is part of a family of proteins that assist in the folding of other partner proteins. These partner proteins are most often upregulated in cancers. Thus, HSP90B1 has recently been considered as a target for the creation of a personalized therapeutic vaccine [59, 60].

The second gene, once more detected at both orders, but at day 8, is GSTP1, which encodes *glutathione S-transferase P1*. This protein protects the cancer tissue from oxygen-reactive stress [61]. Thus, it is in principle one more natural target for therapy. Nonetheless, and unfortunately, no inhibitors of GSTP1 are known to be selective for the cancer cells, which makes a therapeutic strategy based on its inhibition very difficult to create [62].

The most promising finding, however, is the third gene, namely PI3. First of all, with the use of a pairwise network, this gene is only detected in 2 days. However, when using the higher-order network, it is found as significant at all times from day 5 onwards. The gene encodes the protein *peptidase inhibitor 3*, also known as *elafin*, whose action is to specifically block elastases, which are enzymes that break down elastin. The accumulation of elastotic masses is often seen in particular types of aggressive breast cancers, suggesting that their presence positively correlates with the invasiveness of the disease [63]. However, there is conclusive evidence that elafin is downregulated in breast cancer and is involved in the process of tumorigenesis [64, 65]. This seems to indicate that promoting the expression of PI3 could be a viable approach for the treatment of some breast cancers, such as the specific one from which we grew our organoids. This suggestion is made even stronger by the fact that, as mentioned above, the higher-order network detects the importance of this gene continuously, starting from day 5, highlighting the fundamental role of its disruption for the progression of the disease. Notably, to the best of our knowledge, PI3 has not yet been considered as a direct target for cancer therapy, demonstrating the predictive potential of the use of multi-order parenclitic networks.

## IV. CONCLUSIONS

In summary, we have introduced a novel framework for constructing higher-order parenclitic networks, capable of capturing deviations in correlations at any desired order of interaction. We addressed the key challenge of scalability by proposing an efficient approximation scheme that enables practical construction of higher-order structures. It has to be remarked that the approximation becomes increasingly accurate as the dataset size grows.

It should be equally remarked that our method uses no prior information about the system under study at all, and it is thus fundamentally different from approaches based on deep learning and other statistical schemes. In fact, it does not need any training phase, nor does it in-

corporate biases from predefined models or labelled data. This makes it particularly well-suited for exploratory analysis in contexts where mechanistic knowledge is limited or where unbiased discovery is essential.

To test the validity of our method and to showcase its predictive power, we applied it to gene expression levels measured in two sets of organoids, one grown from tissue taken from a mastectomy, and the other from clinically healthy, tumour-adjacent tissue. This allowed us to build two sets of parenclitic hypergraphs. The first provided a comparison between healthy tissue and cancer tissue, and the second yielded a temporal progression of the gene expression anomalies of the cancer.

A major strength of our approach lies in its independence from absolute levels of gene expression, because parenclitic networks actually detect anomalies in the correlations between gene expression levels. Thus, they allow one not only to find single genes that may be overexpressed or underexpressed, but also sets of genes whose overall relationships may be disrupted even if their individual expression is not. Also, the use of higher-order parenclitic networks does not preclude that of traditional ones. In fact, the two are complementary to each other, and the ability, already mentioned above, of extending the method to any order opens the possibility of collecting a significant amount of additional information that is not captured by dyadic networks alone.

The results obtained on the cancer organoids are very intriguing and particularly compelling. First of all, the method detects a large number of known cancer markers, which is effectively an experimental validation of its reliability. Moreover, it also identifies some genes, such as HSP90B1, that are currently under investigation as potential therapeutic targets. Notably, the first suspicions that some heat-shock protein was essential for cancer progression came in 1981 [66], but it was not until 13 years later, in 1994, that its function was actually identified, even though only partially [67], and 10 more years had to pass before the idea of using it as a target for therapeutics was vented [68]. This timeline suggests that parenclitic hypergraphs can significantly accelerate the discovery of clinically relevant targets, potentially shortening the gap between hypothesis and application by years or even decades.

Additionally, our results include at least one new potential therapeutic target, namely elafin, encoded by the PI3 gene. Its relevance is made even more evident by the difference in detection pattern between the pairwise method and the higher-order one. This differential pattern strongly indicates that promoting PI3 expression may significantly slow breast cancer progression.

Finally, a unique advantage of our approach is that the results are inherently patient-specific, since they derive from organoids grown from individual tissue samples. Thus, to the best of our knowledge, this constitutes the first feasible method to generate personalized therapeutic candidates for cancer patients. Given the increasing accessibility of mRNA vaccine technology, offering a safe

and effective means to target specific proteins, we propose parenclitic hypergraphs as a powerful tool for the rapid development of customized therapies, potentially capable of inducing remission even in aggressive cancer types.

## V. METHODS

### A. Synthetic data generation and validation

To generate the synthetic data set used for the first validation of our method, we constructed two populations of 1000 subjects each, with each subject described by 10 features  $f_1$ . The values of the features for the negative-control population were extracted uniformly at random in the interval  $(0, 1)$ , to ensure the absence of any correlation between them. Conversely, the values of the features of the subjects in the positive population were chosen in a way to ensure the existence of three-body correlations amongst the elements of three sets of features.

In particular, the procedure we used is as follows. We first extracted 7 random numbers  $\alpha_i$ , uniformly distributed in  $(0, 1)$ . Then, we put  $f_{10} = \alpha_7$ , and we chose the values of the remaining features so that  $f_1$ ,  $f_2$  and  $f_3$  are functions of  $\alpha_1$  and  $\alpha_2$ ,  $f_4$ ,  $f_5$  and  $f_6$  are functions of  $\alpha_3$  and  $\alpha_4$ , and  $f_7$ ,  $f_8$  and  $f_9$  are functions of  $\alpha_5$  and  $\alpha_6$ . Additionally, we carried out this procedure twice, choosing linear functions in one case and non-linear functions in the other.

Specifically, in the linear case, the functions were

$$f_1 = \alpha_1 \quad (3)$$

$$f_2 = \alpha_2 \quad (4)$$

$$f_3 = \frac{2\alpha_1 + \alpha_2}{3} \quad (5)$$

$$f_4 = \frac{\alpha_3 + \alpha_4}{2} \quad (6)$$

$$f_5 = \frac{\alpha_3 + 2\alpha_4}{3} \quad (7)$$

$$f_6 = \frac{2\alpha_3 + \alpha_4}{3} \quad (8)$$

$$f_7 = \frac{\alpha_5 + \alpha_6}{2} \quad (9)$$

$$f_8 = \frac{\alpha_5 + 3\alpha_6}{4} \quad (10)$$

$$f_9 = \frac{3\alpha_5 + \alpha_6}{4}, \quad (11)$$

Dataset	Subjects	Pathological	Healthy	Features
1 Wisconsin breast cancer	569	212	357	30
2 Parkinson’s disease	195	147	48	22
3 Heart disease	299	138	161	6
4 Coimbra breast cancer	116	64	52	9
5 Indian liver patient records	579	414	165	9

Table I. **Summary of datasets used for validation.**

whereas in the non-linear case, they were

$$f_1 = \frac{\alpha_1^2 + \alpha_2^4}{2} \quad (12)$$

$$f_2 = c_2 (\sin(\alpha_1) + \alpha_2) \quad (13)$$

$$f_3 = c_3 (\alpha_1^3 + \tan(\alpha_2)) \quad (14)$$

$$f_4 = c_4 \alpha_3 e^{\alpha_4 - 1} \quad (15)$$

$$f_5 = c_5 (\ln(\alpha_3 + 1) + \sin(\alpha_4)) \quad (16)$$

$$f_6 = \frac{\alpha_4}{\alpha_3 + 1} \quad (17)$$

$$f_7 = \alpha_6 \cos(\alpha_5) \quad (18)$$

$$f_8 = c_8 \arctan(\alpha_5) \quad (19)$$

$$f_9 = c_9 \sin(\alpha_5 \alpha_6), \quad (20)$$

where we used  $c_2 = 0.543$ ,  $c_3 = 0.391$ ,  $c_4 = 0.3678$ ,  $c_5 = 0.652$ ,  $c_8 = \frac{4}{\pi}$  and  $c_9 = 1.188$ .

## B. Real-world dataset description

From each of the five datasets used to validate our method on real-world data, we first removed all categorical features, if present, since our method relies on continuous numerical values. Then, we discarded any subject with missing values. The resulting data are summarized in Table I. Moreover, we normalized the features, to make them lie in the interval  $[0, 1]$ , using

$$\tilde{f} = \frac{f - \min(f)}{\max(f) - \min(f)} \quad (21)$$

where  $\tilde{f}$  is the rescaled feature value,  $f$  its original value, and the minimum and maximum are taken over all subjects.

In the following, we provide a description of the features used in each data set.

### 1. Breast Cancer Wisconsin (Diagnostic)

The dataset [20, 21] includes features measured from digital images of fine-needle aspirations samples of suspected breast-cancer masses. Each subject is associated to 30 real-valued features, computed from ten distinct nuclear attributes, namely mean radius, standard deviation of grey-scale values (texture), perimeter, area, local

variation in radius (smoothness), compactness, concavity, number of concave points of the contour, symmetry and fractal dimension. For each of these attributes, three values are given, namely their mean and their standard error over all the nuclei found in each image, and the mean of the three largest values in each image, resulting in a comprehensive representation of the nuclear morphology.

### 2. Parkinson’s Disease Detection

Some of Parkinson’s disease’s most typical symptoms are vocal impairments. The dataset [22, 23] comprises 22 voice-derived features, which are: average, maximum and minimum vocal fundamental frequency; absolute and relative jitter of the vocal fundamental frequency; relative amplitude perturbation and five-point period perturbation quotient of the vocal fundamental frequency; average absolute difference of differences between jitter cycles; local shimmer parameter of the vocal fundamental frequency in absolute and logarithmic units; three-point and five-point amplitude perturbation quotient of the shimmer parameter; eleven-point amplitude perturbation quotient of the vocal fundamental frequency; average of absolute differences between the amplitudes of the shimmer parameter in consecutive periods; noise-to-harmonics ratio and harmonics-to-noise ratio of the acoustic signal; recurrence period density entropy; detrended fluctuation value given by the fractal scaling exponent of the signal; two measures of the spread of the vocal fundamental frequency; correlation dimension; recurrence period density entropy.

### 3. Heart Disease

This dataset [24, 25] contains 13 features from 303 subjects. Of these, 7 are categorical (sex, type of chest pain, presence of hyperglycaemia, resting electrocardiographic results, occurrence of exercise-induced angina, sign of the derivative of the peak ST segment during exercise, occurrence of thallium scintigraphic defects during exercise) and were therefore removed from our analysis. The remaining 6 are: age; resting systolic blood pressure; serum cholesterol; maximum heart rate during exercise; ST depression induced by exercise relative to rest; number of major blood vessels colored by fluoroscopy.

#### 4. Breast Cancer Coimbra

The dataset [26, 27] consists of 116 individuals, each described by 9 non-categorical features, namely age, body mass index (BMI), blood glucose, plasma level of insulin, insulin resistance (assessed via the homeostasis model), serum value of leptin, serum value of adiponectin, serum value of resistin and serum value of Monocyte Chemoattractant Protein 1 (MCP-1). The dataset is of particular value for establishing the relationship between metabolic and hormonal biomarkers and breast cancer risk, making it a useful resource for predictive modeling and classification tasks in oncology research.

#### 5. Indian Liver Patients

This dataset [28, 29] consists of 579 individuals with 1 categorical feature (sex) and 9 numerical ones. These are age and values obtained from blood tests: total bilirubin, direct bilirubin, alkaline phosphatase, alanine aminotransferase, aspartate aminotransferase, total proteins, albumin, and the ratio of albumin to globulin. The dataset is widely used for predictive modeling and classification tasks in liver disease research, providing valuable insights into the relationship between biochemical markers and liver health.

### C. Organoid culture

#### 1. Patient tissue and clinical characteristics

Breast tumour and matched tumour-adjacent tissues were obtained from a therapeutic mastectomy and axillary lymph node dissection procedure. The patient was a female diagnosed with a left-sided breast malignancy. Pathological examination of the resection specimen confirmed a 5.2 cm  $\times$  2.5 cm  $\times$  1.6 cm invasive ductal carcinoma (histological grade 3), with 9 of 14 axillary lymph nodes positive for metastasis. Immunohistochemical profiling of the invasive carcinoma revealed ER-positive (60%, strong-moderate), PR-positive (90%, strong-moderate), and HER2-negative status, with a Ki67 proliferation index of 30%.

#### 2. Organoids derivation and culture

Patient-derived organoid models were established as described in Refs. [69] and [70]. In brief, fresh tissues were minced and enzymatically digested in collagenase on an orbital shaker at 37 °C for 1–2 hours. The resulting suspension was filtered through a 100  $\mu$ m strainer, and the cell pellet was collected by centrifugation at 400 rcf. Contaminating red blood cells were lysed via a 5-minute

incubation with a lysis buffer. The purified cell pellet was subsequently resuspended in growth-factor-reduced Matrigel (Corning, #354230), and 40  $\mu$ L drops of the cell-Matrigel suspension were plated in pre-warmed 24-well plates. The drops were allowed to solidify for 20 minutes at 37 °C before being overlaid with organoid culture medium. The culture medium was replaced twice weekly, and organoids were passaged approximately every 2–4 weeks upon reaching 80% confluency within the Matrigel domes using TrypLE™ Express Enzyme (1X), no phenol red (Gibco, #12604013) for dissociation into small clusters. All experiments involving human samples were conducted in compliance with all relevant ethical regulations and were approved by the ethics committees of medical research of the institutions involved. The consent of all subjects has been obtained.

### D. Gene expression data analysis

#### 1. RNA sequencing and data acquisition

To capture dynamic gene expression patterns during organoid development, samples were harvested at seven critical time points, namely days 0, 2, 4, 5, 6, 7 and 8 of the total 9 days of culture. For each sample, total RNA was isolated using RNazol (MRC) based on the manufacturer’s instructions. Bulk RNA-seq library preparation and sequencing were performed at OE Biotech Co., Ltd. (Shanghai, China). To ensure robustness and minimize artifacts, each sample library was sequenced in duplicate.

#### 2. Gene expression data preprocessing

The raw sequencing data yielded two gene expression datasets, one for the tumour-adjacent organoids and one for the breast tumour ones. Initially, the two datasets comprised data for 34415 genes, resulting in an overall dimensionality of  $34415 \cdot 7 = 240905$ , with the maximum expression level recorded over both datasets of 13637 counts. To reduce the effect of noise, before subsequent analyses, we removed from consideration all genes whose expression level was below 30. This left 2381 genes for the cancer organoids and 2431 genes for the healthy ones. Also, we normalized the retained data using Eq. 21.

## VI. AUTHOR CONTRIBUTION

S.B. conceived the study. L.M., G.-Q.S., R.C., M.R., D.P., C.I.D.G., H.G. and S.B. coordinated the research tasks. K.K.H.M. and D.A. developed the parenchymal method and solved the scalability problem. K.K.H.M., D.A. and L.M. developed the code. K.K.H.M., D.A., Y.-J.M. and F.F. performed the tests on synthetic data and real-world data. M.Z., C.C. and J.L. conducted

the organoid experiment and performed genetic measurements on the resulting organoids. F.L., Y.Q., S.Z., Z.Z. and H.G. performed the tests on the genetic data. Y.Q., Y.-J.M. and F.F. prepared the Figures. All authors wrote the manuscript.

## VII. ACKNOWLEDGMENTS

This work is partly supported by the Italian PRIN research project n.2022FHHHPC titled “The structure, dynamics and control of network systems with higher-order interactions”. K.K.H.M. acknowledges support via a PhD scholarship from the Scuola Superiore Meridionale. L.M. gratefully acknowledges the support of the “Hundred Talents” program of the University of Electronic Science and Technology of China, of the “Outstanding Young Talents Program (Overseas)” of the National Natural Science Foundation of China, and of the talent programs of the Sichuan province and Chengdu municipality.

- 
- [1] R. Albert and A.-L. Barabási, *Rev. Mod. Phys.* **74**, 47 (2002).
- [2] M. Newman, *SIAM Rev.* **45**, 2 (2003).
- [3] S. Boccaletti *et al.*, *Phys. Rep.* **424**, 175 (2006).
- [4] S. Boccaletti *et al.*, *Phys. Rep.* **544**, 1 (2014).
- [5] M. E. J. Newman, S. Strogatz and D. J. Watts, *Phys. Rev. E* **64**, 026118 (2001).
- [6] C. I. del Genio, H. Kim, Z. Toroczkai and K. E. Bassler, *PLoS One* **5**, e10012 (2010).
- [7] H. Kim, C. I. del Genio, K. E. Bassler and Z. Toroczkai, *New J. Phys.* **14**, 023012 (2012).
- [8] K. E. Bassler, C. I. del Genio, P. Erdős, I. Miklós and Z. Toroczkai, *New J. Phys.* **17**, 083052 (2015).
- [9] M. Zanin and D. Papo, *Chaos Soliton. Fract.* **138**, 109993 (2020).
- [10] M. Zanin *et al.*, *Sci. Rep.* **4**, 5112 (2014).
- [11] J. H. Martínez *et al.*, *Chaos Soliton. Fract.* **70**, 144 (2015).
- [12] A. Karsakov *et al.*, *PLoS One* **12**, e0169661 (2017).
- [13] M. Zanin, M. Romance, S. Moral and R. Criado, *Complexity* **2018**, 5764370 (2018).
- [14] H. J. Whitwell, O. Blyuss, U. Menon, J. F. Timms and A. Zalkin, *Oncotarget* **9**, 22717 (2018).
- [15] T. Nazarenko, H. J. Whitwell, O. Blyuss and A. Zalkin, *Front. Genet.* **12**, 733783 (2021).
- [16] H. Zhang, T. Oyelade, K. P. Moore, S. Montagnese and A. R. Mani, *Front. Netw. Physiol.* **2**, 833119 (2022).
- [17] M. Krivonosov *et al.*, *Chaos Soliton. Fract.* **165**, 112863 (2022).
- [18] F. Battiston *et al.*, *Phys. Rep.* **874**, 1 (2020).
- [19] S. Boccaletti *et al.*, *Phys. Rep.* **1018**, 1 (2023).
- [20] W. N. Street, W. H. Wolberg and O. L. Mangasarian, *Proceedings of the IS&T/SPIE 1993 International Symposium on Electronic Imaging Science and Technology* **1905**, 861 (1993).
- [21] <https://doi.org/10.24432/C5DW2B>
- [22] M. A. Little, P. E. McSharry, S. J. Roberts, D. A. E. Costello and I. M. Moroz, *Biomed. Eng. Online* **6**, 23 (2007).
- [23] <https://doi.org/10.24432/C59C74>
- [24] R. Detrano *et al.*, *Am. J. Cardiol.* **64**, 304 (1989).
- [25] <https://doi.org/10.24432/C52P4X>
- [26] M. Patrício *et al.*, *BMC Cancer* **18**, 29 (2018).
- [27] <https://doi.org/10.24432/C52P59>
- [28] A. Gulia, R. Vohra and P. Rani, *Int. J. Comput. Sci. Inf. Technol. Res.* **5**, 5110 (2014).
- [29] <https://doi.org/10.24432/C5D02C>
- [30] E. V. Bandera and E. M. John, *JAMA Oncology* **4**, 804 (2018).
- [31] K. Liu *et al.*, *Cancer Manag. Res.* **10**, 143 (2018).
- [32] N. Tzenios, M. E. Tazanios and M. Chahine, *Medicine* **103**, e36831 (2023).
- [33] C. Dauccia *et al.*, *Breast*, *in press*, [https://www.thebreastonline.com/article/S0960-9776\(26\)00020-2/fulltext](https://www.thebreastonline.com/article/S0960-9776(26)00020-2/fulltext)
- [34] Z. Zhao *et al.*, *Nat. Rev. Methods Primers* **2**, 94 (2022).
- [35] N. L. G. Y. Komalasari *et al.*, *Front. Oncol.* **13**, 1142907 (2023).
- [36] M. P. Chao *et al.*, *Science Transl. Med.* **2**, 63ra94 (2010).
- [37] G. Claps *et al.*, *Nat. Rev. Clin. Oncol.* **19**, 749 (2022).
- [38] A.-X. Guo, J.-J. Cui, L.-Y. Wang and J.-Y. Yin, *Cell Commun. Signal.* **18**, 14 (2020).
- [39] J. Lv *et al.*, *Science Transl. Med.* **15**, eabq6024 (2023).
- [40] U. Schlattner *et al.*, *Biophys. J.* **121**, 510A (2022).
- [41] T. Wiedl *et al.*, *J. Proteom.* **74**, 1884 (2011).
- [42] R. Kumari *et al.*, *Br. J. Cancer* **124**, 1428 (2021).
- [43] Y. Yang *et al.*, *Cell. Mol. Biol. Lett.* **26**, 50 (2022).
- [44] C. Shen, J. Zhuo and J. Wang, *Sci. Rep.* **15**, 26111 (2025).
- [45] B. Hu, G. Yin and X. Sun, *Sci. Rep.* **12**, 10231 (2022).
- [46] A. Filipek, V. Gerke, K. Weber and J. Kuznicki, *Eur. J. Biochem.* **195**, 795 (1991).
- [47] H. Akiyama, *Mod. Rheumatol.* **18**, 213 (2008).
- [48] M. J. Barter *et al.*, *Development* **144**, 4510 (2017).
- [49] A. Tariq *et al.*, *RNA* **26**, 175 (2020).
- [50] S. Jia *et al.*, *Oncolog.* **29**, e25 (2024).
- [51] Y. Wang *et al.*, *Front. Mol. Biosci.* **10**, 1157970 (2023).
- [52] D. A. Guertin and D. M. Sabatini, *Trends Mol. Sci.* **8**, P353 (2005).
- [53] J. B. Easton and P. J. Houghton, *Oncogene* **25**, 6436 (2006).
- [54] K. Xu, P. Liu and W. Wei, *Biochim. Biophys. Acta Rev. Cancer* **1846**, 638 (2014).
- [55] J. M. Dolezal, A. P. Dash and E. V. Prochownik, *BMC Cancer* **18**, 275 (2018).
- [56] H. Lu *et al.*, *Open Med.* **16**, 1 (2020).
- [57] M. Lengyel *et al.*, *Cancer Sci.* **116**, 81 (2024).
- [58] S. C. Akincilar, C. H. T. Chan, Q. F. Ng, K. Fidan and V. Tergaonkar, *Cell. Mol. Life Sci.* **78**, 4235 (2021).

- [59] C. G. Wood and P. Mulders, *Fut. Oncol.* **5**, 763 (2009).
- [60] G. Tosti, A. di Pietro, P. F. Ferrucci and A. Testori, *Exp. Rev. Vacc.* **8**, 1513 (2014).
- [61] X. Dong *et al.*, *Cell Death Diff.* **26**, 2086 (2019).
- [62] B. O. Al-Najjar, M. Helal, F. G. Saqallah and B. Bandy, *RCS Med. Chem.* **16**, 1516 (2025).
- [63] S. Salesse *et al.*, *FEBS Open Bio.* **8**, 1395 (2018).
- [64] K. K. Hunt *et al.*, *Breast Cancer Res.* **15**, R3 (2013).
- [65] J. A. Caruso *et al.*, *Breast Cancer Res.* **16**, 3417 (2014).
- [66] H. Oppermann, W. Levinson and J. M. Bishop, *Proc. Natl. Acad. Sci. USA* **78**, 1067 (1981).
- [67] L. Whitesell, E. G. Mimnaugh, B. De Costa, C. E. Myers and L. M. Neckers, *Proc. Natl. Acad. Sci. USA* **91**, 8324 (1994).
- [68] J. S. Isaacs, W. Xu and L. Neckers, *Cancer Cell* **3**, 213 (2003).
- [69] J. F. Dekkers *et al.*, *Nat. Protoc.* **16**, 1936 (2021).
- [70] N. Sachs *et al.*, *Cell* **172**, 373 (2018).